



**The Abdus Salam
International Centre for Theoretical Physics**



2060-55

**Advanced School on Non-linear Dynamics and Earthquake
Prediction**

28 September - 10 October, 2009

Asymmetric ocean basins

C. Doglioni
*Dipartimento di Scienze della Terra
Università La Sapienza
Rome
Italy*

1 Asymmetric ocean basins

2 **Giuliano Panza¹, Carlo Doglioni², and Anatoli Levshin³**

3 *¹Dipartimento di Scienze della Terra, Università di Trieste, 34127 Trieste, and ICTP Trieste*
4 *Italy*

5 *²Dipartimento di Scienze della Terra, Università Sapienza, & CNR-IGAG, 00185 Roma, Italy*

6 *³Department of Physics, University of Colorado, Boulder, CO 80309, USA*

7 **ABSTRACT**

8 While the superficial expression of oceanic ridges is generally symmetric, their deeper
9 roots may be asymmetric. Based on a surface-wave tomographic 3D model of the Earth's upper
10 300 km, we construct a global cross-section parallel to the equator of the net-rotation of the
11 lithosphere, the so-called tectonic equator. Shear wave velocities indicate a difference between
12 the western and eastern flanks of the three major oceanic rift basins (Pacific, Atlantic and Indian
13 ridges). In general, the western limbs have a faster velocity and thicker lithosphere relative to the
14 eastern or northeastern one, whereas the upper asthenosphere is faster in the eastern than in the
15 western limb. We interpret the difference among the two flanks as the combination of mantle
16 depletion along the oceanic rifts and of the "westward" migration of the ridges and the
17 lithosphere relative to the mantle. The low-velocity zone (LVZ) in the upper asthenosphere at the
18 depth of 120–200 km is assumed to represent the decoupling between the lithosphere and the
19 underlying mantle. It is also well defined by the distribution of radial anisotropy that reaches
20 minimum values close to the rifts, but with an eastward offset. These results could be explained
21 in the frame of the "westward" drift of the lithosphere relative to the underlying mantle.

22 **INTRODUCTION**

23 The mantle is thought to rise adiabatically along oceanic ridges and to melt, generating
24 new oceanic crust (e.g., Cann et al., 1999 and references therein). Since the recognition of
25 magnetic anomalies on both sides of the ridges, oceanic basins have generally been associated to
26 symmetric spreading. However, it has been shown that rift zones are moving on the Earth's
27 surface relative to the underlying mantle, i.e., they are decoupled with respect to the mantle.
28 Plate boundaries move to the west relative to Antarctica and to the hotspot reference frame (e.g.,
29 Le Pichon, 1968, Garfunkel et al., 1986).

30 In fact, a number of papers have described some asymmetric spreading, differences in
31 geometry and subsidence between the two ridge, as well as heterogeneities in the underlying
32 mantle tomography (e.g., Morgan and Smith, 1992; Zhang and Tanimoto, 1993; Calcagno and
33 Cazenave, 1994; Cande and Kent, 1995; Bonatti et al., 2003; Pilidou et al., 2005; Muller et al.
34 2008).

35 Subduction zones show a marked asymmetry as a function of their geographic polarity
36 (Doglioni et al., 2007); in this research we tested whether a worldwide asymmetry holds for
37 oceanic rifts as well.

38 For this purpose, we extracted sections across the S-wave tomographic model of the
39 Earth's lithosphere-asthenosphere system (Shapiro and Ritzwoller, 2002). The sections are
40 perpendicular to the three main oceanic ridges, i.e., East Pacific Rise (EPR), Mid Atlantic Ridge
41 (MAR) and Indian Ridge (IR), as shown in Figure 1. The first global cross-section coincides
42 with the so-called "tectonic equator" (TE), which is the ideal line along which plates move over
43 the Earth's surface with the fastest mean angular velocity toward the "west" relative to the
44 mantle (Crespi et al., 2007). The coordinates of the sections are in Table 1 of the data repository.

45 **3-D SHEAR VELOCITY MODEL**

46 We considered a 3D shear velocity model of the Earth's upper mantle, CUB2 (Shapiro
47 and Ritzwoller, 2002; <http://ciei.colorado.edu/~nshapiro/MODEL>) obtained by tomographic
48 inversion of seismic surface waves generated by earthquakes and recorded by numerous seismic
49 stations across the world. It provides a quite detailed (at 2° by 2° geographical grid) shear-wave
50 velocity (V_s) image of the uppermost 300 km of the Earth. This model is the result of the Monte-
51 Carlo inversion of dispersion data-group velocities of fundamental Rayleigh and Love modes, in
52 the range of periods 16–200s (Levshin et al., 1989; Ritzwoller and Levshin, 1998; Ritzwoller et
53 al., 2002[[Not in reference list?]]) and phase velocities, in the range of period 40–200s,
54 (Trampert and Woodhouse, 1995, and Ekstrom et al., 1997). The procedure allows for the
55 recognition of the radial anisotropy of shear velocities in the upper mantle down to 220 ± 30 km
56 depth and provides estimates of the uncertainty in the inversion.

57 To obtain V_s radial cross-sections across this model we use bispline interpolation of
58 velocities at fixed depths levels (on a 4 km grid) with subsequent gaussian smoothing. Here the
59 V_s is taken here as an average of V_{sv} and V_{sh} along two sections (tectonic equator, TE, and along
60 a sort of perturbed tectonic equator, TE-pert), covering 10° width (Fig. 1). The magnitude of the
61 radial anisotropy $(V_{sh}-V_{sv})/V_s$ predicted by the model is shown in Figure 1.

62 Another section slightly deviates from the TE, along a sort of perturbed tectonic equator
63 (TE-pert). Along the TE-pert, following a sort of funneling, the low-velocity layer (LVZ),
64 corresponding to the upper asthenosphere, has shear wave velocity lower than 4.5 km/s
65 everywhere, i.e., all across the Earth at a depth of ~ 130 –200 km.

66 The V_s model shows an asymmetry in the uppermost 100 km between the western side
67 (4.5–4.8 km/s), which is faster with respect to the eastern side of the rift (4.4–4.6 km/s). The
68 upper asthenosphere (100–200 km) of the western flank is slow ($V_s = 4.2$ –4.4 km/s) compared to

69 the eastern flank ($V_s = 4.3\text{--}4.5$ km/s). Therefore, the difference in V_s between the western and
70 the eastern flanks of the rift, both in the lithosphere and in the asthenosphere, is significant and in
71 the range of 0.1–0.3 km/s. The LVZ shows an asymmetric pattern, it is deeper and thicker on the
72 west than on the east side of the ridge. This is particularly evident in the Eastern Pacific Ridge
73 (EPR). In the western lithosphere of the Mid Atlantic Ridge (MAR) the V_s horizontal gradient is
74 much larger than the one in EPR, in agreement with the slower spreading rate of the MAR.

75 **GEODYNAMIC MODEL**

76 The bathymetry of rift zones is, in general, asymmetric: the eastern flank is in average
77 slightly shallower (100–300 m) than the western flank (Doglioni et al., 2003). See Fig. A in the
78 data repository. Since the mantle becomes depleted in Fe when it melts beneath a ridge (Oxburgh
79 and Parmentier, 1977), and it moves “eastward” relative to the lithosphere, the shallower
80 bathymetry to the east has been interpreted in terms of an isostatic adjustment, i.e., a lower
81 thermal subsidence in the eastern flank of the ridge (Doglioni et al., 2005). Due to the net
82 rotation of the lithosphere (Gripp and Gordon, 2002; Crespi et al., 2007; Husson et al., 2008), the
83 subridge depleted and lighter mantle will eventually transit beneath a continent to the east, if any,
84 and uplifting it (e.g., Africa, Doglioni et al., 2003).

85 Since rifts show a difference that appears to be chiefly controlled by the geographical
86 distribution of the anomalies (V_s , bathymetry), we interpret the asymmetry in terms of the
87 “westward” drift of the lithosphere relative to the mantle (Scoppola et al., 2006), along the
88 tectonic equator (TE) of Crespi et al. (2007), which makes an angle of $\sim 30^\circ$ relative to the
89 geographic equator.

90 The hot mantle rising along ridges is decompressed, thus melts and delivers fluids. This
91 process determines a chemical depletion of the pre-melting mantle: the residual mantle

92 undergoes a modification of its physical properties, such as the decrease in density ($20\text{--}60\text{ kg/m}^3$,
93 Oxburg and Parmentier, 1977[[[Oxburg or Oxburgh? See reference list as well.](#)]]) and
94 consequent natural increase of V_s due to Fe depletion, increase of 1–2 orders of magnitude of
95 viscosity and temperature decrease of around $100\text{ }^\circ\text{C}$. At shallower lithospheric depths, in the
96 range $0\text{--}80\text{ km}$, due to cooling and associated with its westward motion relative to the underlying
97 mantle, the lithosphere is forming from depleted mantle, and has naturally lower velocities than
98 on the western side of the ridge.

99 Ridges move relative to the mantle, with velocity V_r given by $(V_a+V_b)/2$, where V_a and
100 V_b are the velocities relative to the mantle of the two plates (a) and (b), separated by the rift. The
101 ridge is the seat of mantle depletion due to melting, to form new oceanic crust (Fig. 2). The
102 melting region of the mantle gradually shifts westward, affecting new sections of undepleted
103 mantle. This process delivers depleted mantle to the eastern side of the rift. In other words, the
104 residual asthenosphere shifts “eastwards”, with the upper part cooled to form the lithospheric
105 mantle of the eastern flank. Therefore, the ridge is permanently transiting “westward” over a
106 “fertile” mantle able to steadily supply MORB melts. However, once transited, there will be a
107 compositional depletion in the mantle that should appear when comparing the
108 lithosphere/asthenosphere of the western side of the rift with its eastern conjugate counterpart.
109 This would explain the difference in V_s observed at both sides of the rift.

110 Zoomed-in images of cross-sections along the TE at rift zones (EPR, MAR, IR) show this
111 asymmetry (Fig. 3). In order to test whether this observation is a local occasional asymmetry, a
112 number of sections perpendicular and parallel to the ridge have been constructed along TE (Fig.
113 3) and far away from it (Figs. B, C and D in the data repository). They are still supportive an

114 asymmetric pattern in the upper mantle when comparing the western and the eastern sides of the
115 rift, particularly in the Pacific and Indian ridges.

116 Similarly, a slower asthenosphere in the western side of the EPR has been identified in
117 the Melt experiment, interpreted as due to more pronounced melting in the western
118 asthenospheric mantle (e.g., Scheirer et al., 1998). There are areas where this asymmetry is not
119 evident, or possibly sections where it is even reverse. However, it appears as a dominant feature.

120 The partial melting in the mantle beneath ridges varies as a function of a number of
121 parameters, such as the tectonic setting (e.g., smaller along transtensive rifts), the original mantle
122 composition and fluids content, the temperature of the mantle, etc. The variation in V_s is by
123 definition associated to the variation of the square root of the ratio between rigidity (μ) and
124 density (ρ). However it remains unsolved, at least to our knowledge, how to relate in detail the
125 variation of those parameters with the mantle modification at ridges. Oxburg and Parmentier
126 (1977) suggested that there is mantle depletion along ridges, regardless the rift is symmetric or
127 asymmetric. From tomography images (see also Pilidou et al. 2005), all we can say is that the
128 ratio μ/ρ is different between at the two sides of the ridges. Moreover the mean bathymetry is
129 slightly shallower in the eastern flank of the rifts. Therefore, due to the westerly migration of
130 ridges and of the lithosphere relative to the underlying mantle, we propose to interpret the
131 asymmetry as the result of an oblique upraising of the mantle and the distribution of the related
132 depletion.

133 **RADIAL ANISOTROPY**

134 Detailed information on the seismic anisotropy of the Earth's mantle provides insight into
135 paleo and recent deformation processes and therefore mantle dynamics. Radial anisotropy of
136 shear velocities in the upper mantle is usually characterized by the ratio $\eta = (V_{sh}-V_{sv})/V_s$,%

137 where V_{sh} and V_{sv} are velocities of two types of shear waves of different polarization and $V_s =$
138 $(V_{sh} + V_{sv})/2$.

139 In the anisotropy sections, both along TE and TE-pert, the minimum value of radial
140 anisotropy is reached, in general at a depth of ~ 200 km, with outstanding exceptions in proximity
141 of the ridges. The level at which radial anisotropy is low, say below 1%, may well represent the
142 decoupling level between the lithosphere and the underlying asthenospheric LVZ, due to the
143 presence of a relevant fraction of melt that inhibits the formation of preferential orientations in
144 the texture of mantle rocks. In particular, along TE-pert very low values of radial anisotropy ($<$
145 1%) reach the top of the section (20 km below surface) with an eastward shift of $\sim 20^\circ$ with
146 respect to EPR and MAR, and a smaller shift is seen along TE, with respect to EPR, all in
147 agreement with the notion of westward drift of the lithosphere relative to the underlying mantle
148 (first order flow). From Figure 1 one can infer that the shift between the geographical ridges axis
149 and the vertical stripes of radial anisotropy $< 1\%$ - the "anisotropy ridge" - axis varies from
150 ~ 1250 km to 2500 km (eastward). The formation of a sizeable solid lid at the ridge sides requires
151 not more than 10–20 My (e.g., Leeds et al., 1974; Forsyth, 1975; Panza, 1980) and both a
152 systematic increase in velocities with the age of the seafloor and anisotropy of propagation are
153 observed (Forsyth, 1975). From the above values one gets an average westward lithosphere
154 velocity of ~ 12.5 cm/y. This value is the result of the ratio between the extremes of the space and
155 time intervals.

156 The exception of MAR along TE section, is only apparent; in fact, the relatively high
157 radial anisotropy there can be explained by the fact that TE intersects the MAR where the ridge
158 makes an almost 90° bend, thus giving rise to apparent anisotropy, related to geometry rather
159 than rock texture.

160 **DISCUSSION AND CONCLUSIONS**

161 We show relevant horizontal Vs variations both in the lithosphere (uppermost say 100 km
162 of the Earth) and in the upper asthenosphere (LVZ, from say 100–200 km of depth). However,
163 the LVZ in the upper asthenosphere is recognized all across the Earth as a persistent layer at the
164 depth of 120–200 km, as shown in a modified path of the tectonic equator. Across rift zones the
165 main velocity variation is of the order of 0.1–0.3 km/s, where the western flank has a faster
166 lithosphere and a slower asthenosphere relative to the eastern or northeastern flank. Whatever the
167 cause, rift zones show a worldwide mean signature in terms of asymmetry, with a stronger Vs
168 contrast between lithosphere and asthenosphere in the western limb when compared to the
169 eastern one. We interpret it as the depletion of the asthenosphere along the rift, while the ridge is
170 moving “westward” relative to the mantle. The lithosphere to the east would represent the
171 cooling of the more depleted asthenosphere, abandoned after the ridge migration to the west.
172 This process is consistent with the net rotation of the lithosphere relative to the underlying
173 mantle. This decoupling is postulated by the sizeable amount of melting that can be inferred from
174 Vs and radial anisotropy sections at ~190–220 km (Fig. 1). In this interpretation, beneath the
175 decoupling, the mantle shifts “eastward” relative to the lithosphere (first order flow). This
176 relative motion could be responsible for the main anisotropy recorded by shear-wave splitting
177 analysis (e.g., Debayle et al. 2005). Along ridges, the oblique rising mantle could be responsible
178 for the asymmetric pattern (second order flow, Fig. 4). The heterogeneity among the flanks of
179 ocean basins mirrors the differences of subduction zones as a function of their geographic
180 polarity. This polarization along the tectonic equator points to an asymmetric Earth, as expected
181 for a complete net rotation of the lithosphere (1.20°/Myr, Crespi et al., 2007).

182 **ACKNOWLEDGMENTS**

183 Discussions with E. Carminati, M. Cuffaro, D. Forsyth, F. Innocenti and F. Riguzzi
184 were very helpful. The article benefited by the critical review of Enrico Bonatti, L. Husson
185 and two anonymous referees and constructive criticisms by the editor S.J. Wyld. The authors
186 highly appreciate the opportunity to have access to the tomographic model CUB2 by Nikolai
187 Shapiro and Michael Ritzwoller. Parts of figures have been plotted using GMT (Wessel and
188 Smith, 1995). M. Cuffaro provided technical support.

189 **REFERENCES CITED**

- 190 Bonatti, E., et al., 2003, Mantle thermal pulses below the Mid-Atlantic Ridge and temporal
191 variations in the formation of oceanic lithosphere: *Nature*, v. 423, p. 499–505, doi:
192 10.1038/nature01594.
- 193 Calcagno, P., and Cazenave, A., 1994, Subsidence of the seafloor in the Atlantic and Pacific
194 oceans; regional and large-scale variations: *Earth and Planetary Science Letters*, v. 126,
195 no. 4, p. 473–492, doi: 10.1016/0012-821X(94)90125-2.
- 196 Cande, S.C. and Kent, D.V., 1995, Revised calibration of the geomagnetic polarity timescale for
197 the Late Cretaceous and Cenozoic: *Journal of Geophysical Research*, B, v. 100/4, p. 6093–
198 6095.
- 199 Cann, J.R., Elderfield, H., and Laughton, A.S., eds., 1999, *Mid-Ocean Ridges, Dynamics of*
200 *Processes Associated with the Creation of New Oceanic Crust*. Cambridge University Press,
201 p. 301.
- 202 Crespi, M., Cuffaro, M., Doglioni, C., Giannone, F., and Riguzzi, F., 2007, Space geodesy
203 validation of the global lithospheric flow: *Geophysical Journal International*, v. 168, p. 491–
204 506, doi: 10.1111/j.1365-246X.2006.03226.x.

- 205 Debayle, E., Kennett, B., and Priestley, K., 2005, Global azimuthal seismic anisotropy and the
206 unique plate-motion deformation of Australia: *Nature*, v. 433, p. 509–512, doi:
207 10.1038/nature03247.
- 208 Doglioni, C., Carminati, E., and Bonatti, E., 2003, Rift asymmetry and continental uplift:
209 *Tectonics*, v. 22, no. 3, p. 1024, doi: 10.1029/2002TC001459.
- 210 Doglioni, C., Green, D., and Mongelli, F., 2005, On the shallow origin of hotspots and the
211 westward drift of the lithosphere: in *Plates, Plumes and Paradigms*, G.R. Foulger, J.H. et al.,
212 *Geol. Soc. Am. Spec. Paper* v. 388, p. 735–749.
- 213 Doglioni, C., Carminati, E., Cuffaro, M., and Scrocca, D., 2007, Subduction kinematics and
214 dynamic constraints: *Earth-Science Reviews*, v. 83, p. 125–175, doi:
215 10.1016/j.earscirev.2007.04.001.
- 216 Gripp, A.E., and Gordon, R.G., 2002, Young tracks of hotspots and current plate Velocities:
217 *Geophysical Journal International*, v. 150, p. 321–361, doi: 10.1046/j.1365-
218 246X.2002.01627.x.
- 219 Ekstrom, G., Tromp, J., and Larson, E.W.F., 1997, Measurements and global models of surface
220 wave propagation: *Journal of Geophysical Research*, v. 102, p. 8137–8157, doi:
221 10.1029/96JB03729.
- 222 Forsyth, D.W., 1975, The early structural evolution and anisotropy of the oceanic upper mantle:
223 *Geophysical Journal of the Royal Astronomical Society*, v. 43, p. 103–162.
- 224 Garfunkel, Z., Anderson, C.A., and Schubert, G., 1986, Mantle circulation and the lateral
225 migration of subducted slabs: *Journal of Geophysical Research*, v. 91, B7, p. 7205–7223,
226 doi: 10.1029/JB091iB07p07205.

- 227 Husson, L., Conrad, C.P., and Faccenna, C., 2008, Tethyan closure, Andean orogeny, and
228 westward drift of the Pacific Basin: *Earth and Planetary Science Letters*, v. 271, p. 303–310,
229 doi: 10.1016/j.epsl.2008.04.022.
- 230 Leeds, A.R., Knopoff, L., and Kausel, E., 1974, Variations of upper mantle structure under the
231 Pacific ocean: *Science*, v. 186, p. 141–143, doi: 10.1126/science.186.4159.141.
- 232 Le Pichon, X., 1968, Sea-floor spreading and continental drift: *Journal of Geophysical Research*,
233 v. 73, no. 12, p. 3661–3697, doi: 10.1029/JB073i012p03661.
- 234 Levshin, A.L., Yanovskaya, T.B., Lander, A.V., Bukchin, B.G., Barmin, M.P., Ratnikova, L.I.,
235 and Its, E.N., 1989, *Seismic Surface Waves in Laterally Inhomogeneous Earth: (Ed. V.I.
236 Keilis-Borok)*, Kluwer Publ. House.
- 237 Morgan, J.P., and Smith, W.H.E., 1992, Flattening of the sea-floor depth-age curve as a response
238 to asthenospheric flow: *Nature*, v. 359, p. 524–527, doi: 10.1038/359524a0.
- 239 Müller, R.D., Sdrolias, M., Gaina, C., and Roest, W.R., 2008, Age, spreading rates and spreading
240 asymmetry of the world's ocean crust: *Geochemistry Geophysics Geosystems*, v. 9,
241 p. Q04006, doi: 10.1029/2007GC001743.
- 242 Oxburgh, E.R., and Parmentier, E.M., 1977, Compositional and density stratification in oceanic
243 lithosphere; causes and consequences: *Journal of the Geological Society*, v. 133, no. 4,
244 p. 343–355, doi: 10.1144/gsjgs.133.4.0343.
- 245 Panza, G.F., 1980, *Evolution of the Earth's lithosphere*. NATO Adv. Stud. Inst. Newcastle, 1979.
246 In: *Mechanisms of Continental Drift and Plate Tectonics*. Ed. by: P.A. Davies and S.K.
247 Runcorn, Academic Press, 75–87.

- 248 Pilidou, S., Priestley, K., Debayle, E., and Gudmundsson, O., 2005, Rayleigh wave tomography
249 in the North Atlantic: high resolution images of the Iceland, Azores and Eifel mantle
250 plumes: *Lithos*, v. 79, p. 453–474, doi: 10.1016/j.lithos.2004.09.012.
- 251 Ritzwoller, M.H., and Levshin, A.L., 1998, Eurasian surface wave tomography: Group
252 velocities: *Journal of Geophysical Research*, v. 103, p. 4839–4878, doi: 10.1029/97JB02622.
- 253 Scheirer, D.S., Forsyth, D.W., Cormier, M.H., and Macdonald, K.C., 1998, Shipboard
254 geophysical indications of asymmetry and melt production beneath the East Pacific Rise
255 near the MELT experiment: *Science*, v. 280, p. 1221–1224, doi:
256 10.1126/science.280.5367.1221.
- 257 Scoppola, B., Boccaletti, D., Bevis, M., Carminati, E., and Doglioni, C., 2006, The westward
258 drift of the lithosphere: a rotational drag?: *Geological Society of America Bulletin*, v. 118,
259 no. 1/2, p. 199–209, doi: 10.1130/B25734.1.
- 260 Shapiro, N.M., and Ritzwoller, M.H., 2002, Monte-Carlo inversion for a global shear velocity
261 model of the crust and upper mantle: *Geophysical Journal International*, v. 151, p. 88–105,
262 doi: 10.1046/j.1365-246X.2002.01742.x.
- 263 Trampert, J., and Woodhouse, J.H., 1995, Global phase velocity maps of Love and Rayleigh
264 waves between 40 and 150 s: *Geophysical Journal International*, v. 122, p. 675–690, doi:
265 10.1111/j.1365-246X.1995.tb07019.x.
- 266 **[[Not cited?]]**Wessel, P.A., and Smith, W.H., 1995, New version of the Generic Mapping Tools
267 released: *Eos, Transactions, American Geophysical Union*, v. 76, Suppl., p. 329, doi:
268 10.1029/95EO00198.

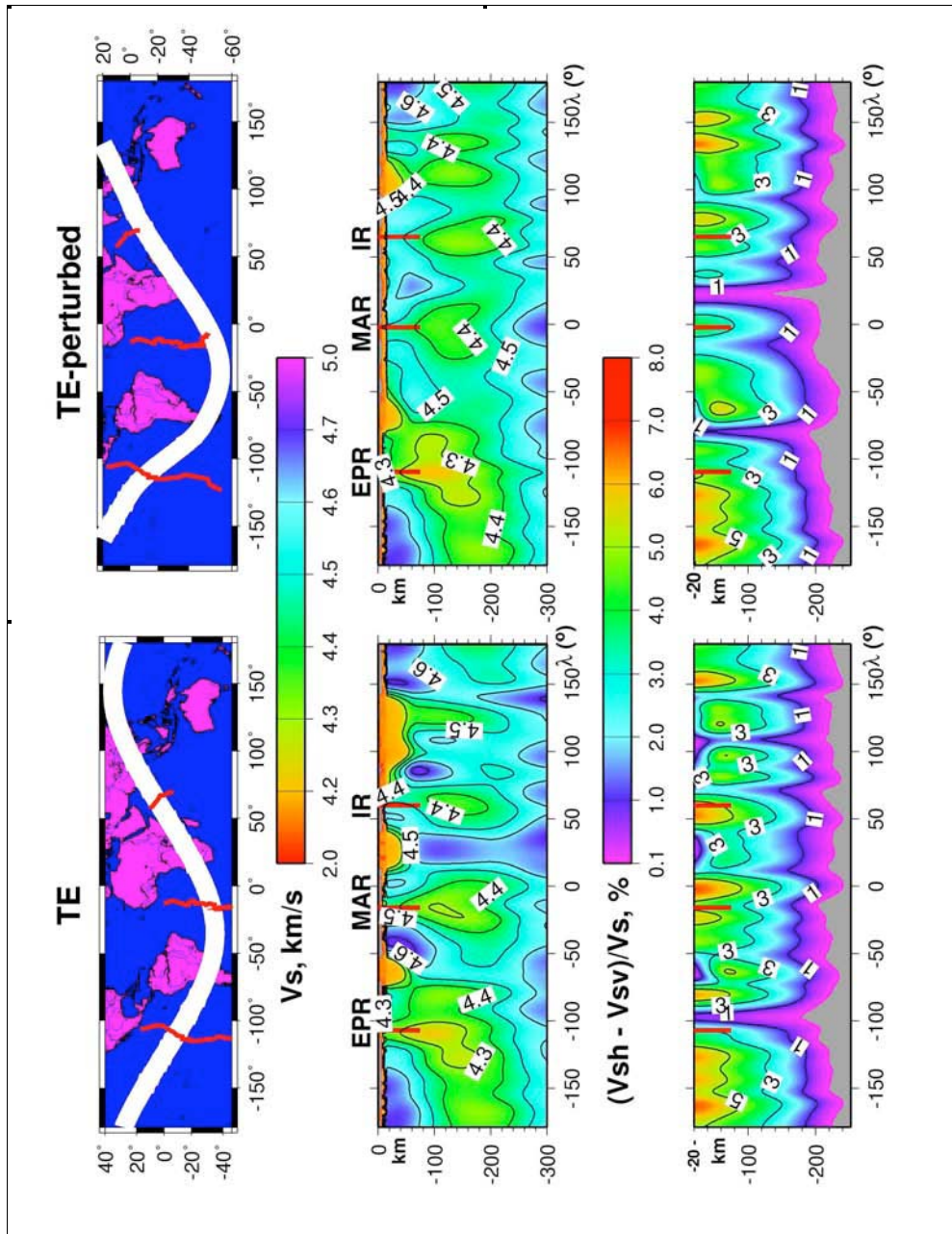
Publisher: GSA
Journal: GEOL: Geology
Article ID: G30570

269 Zhang, Y.S., and Tanimoto, T., 1993, High-Resolution Global Upper Mantle Structure and Plate
270 Tectonics: Journal of Geophysical Research, v. 98, B6, p. 9793–9823, doi:
271 10.1029/93JB00148.

272 **FIGURE CAPTIONS**

273

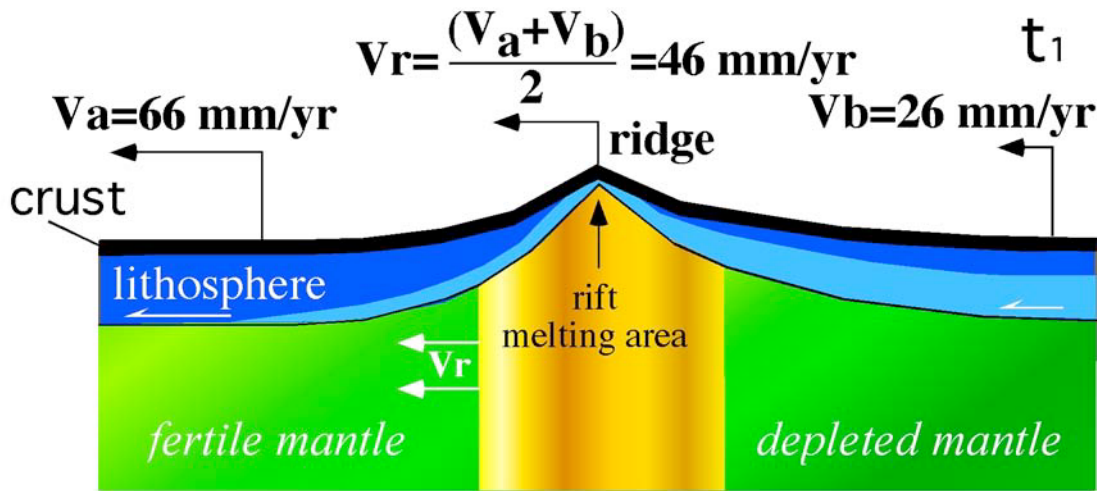
274



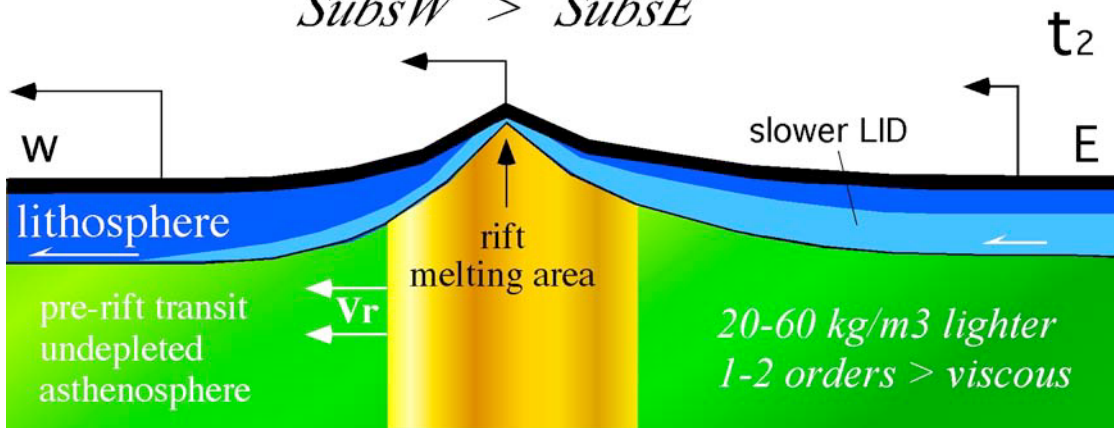
275

276 Figure 1. Shear-wave Earth's section along the tectonic equator (TE) proposed by Crespi et al.
 277 (2007) to the left, and along a perturbed path (TE-pert). Note the generalized asymmetry across
 278 oceanic ridges: the lithosphere (0–100 km) in the western side of the rift is faster than in the
 279 eastern or northeastern side, whereas the upper asthenosphere (LVZ, 100–200 km) is slower in
 280 the western side with respect to the conjugate counterpart. Red lines correspond to elements of
 281 Eastern Pacific, Mid Atlantic and Indian ridges. The lower panels show the radial anisotropy
 282 along these sections. To obtain Vs radial cross-sections we used bispline interpolation of
 283 velocities at fixed depths levels (on a 4 km grid) with subsequent gaussian smoothing. The Vs is
 284 taken here as an average of Vsv and Vsh along a section covering 10° width. The radial
 285 anisotropy sections are without crust, since crust is assumed isotropic.

286

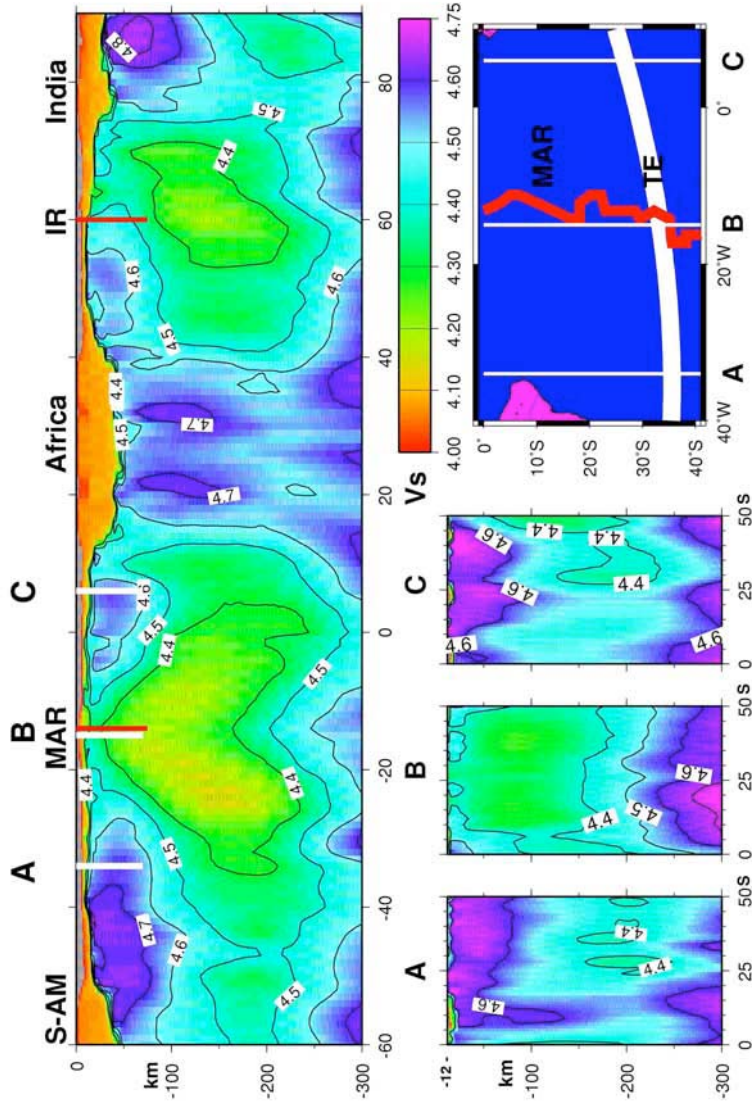


spreading rate 40 mm/yr
Subs_W > Subs_E

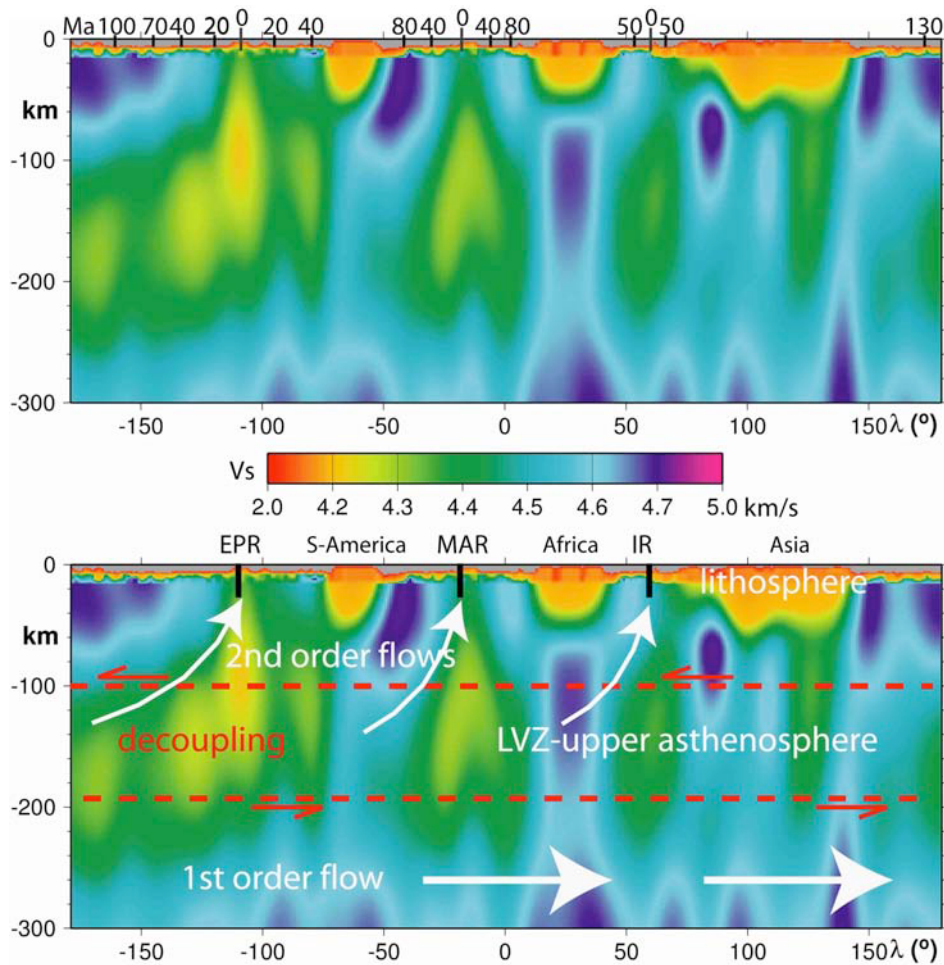


287

288 Figure 2. Cartoon of an oceanic rift with hypothetical velocities of plates a and b relative to the
 289 fixed mantle. The ridge moves west at the velocity of the ridge (V_r). The separation between
 290 plates triggers the uplift of undepleted mantle previously located to the west. In the melting area,
 291 the mantle loses Fe, Mg, and other minerals to form oceanic crust, while the residual mantle is
 292 depleted. Since the melting area moves west it gradually transits toward the undepleted mantle,
 293 releasing to the east a depleted mantle. This can explain the slightly shallower bathymetry of the
 294 eastern limb, but it should also generate an asymmetry of seismic waves velocity seen in Figure
 295 1. In this model, the differential velocity among plates is controlled by LVZ viscosity variations
 296 generating variable decoupling between the lithosphere and the mantle. Modified after Dogliani
 297 et al. (2005).
 298



299
300 Figure 3. Above, enlarged shear-wave cross-section of the Mid Atlantic and the Indian ridges
301 along the tectonic equator (TE). Unlike Figure 1, the velocities are unsmoothed. A-B-C are N-S
302 cross-sections parallel to the southern Mid Atlantic ridge (see small map with MAR in red). The
303 western side of the ridge shows faster lithosphere and slower asthenosphere, both moving
304 perpendicularly and parallel to the ridge. Data from CUB2 model, see text.
305
306



307
308 Figure 4. Uninterpreted (above) and interpreted sections along the tectonic equator of the Earth's
309 first 300 km. The upper asthenosphere contains the LVZ, i.e., what is supposed to be the main
310 decoupling surface between the lithosphere and the mantle, allowing the net rotation of the
311 lithosphere, i.e., the first order relative "eastward" relative mantle flow, or "westward" drift of
312 the lithosphere. Secondary flow should be related to the mantle obliquely upraised along oceanic
313 ridges. The asymmetry among the two sides of the ridges is independent from the age of the
314 oceanic lithosphere shown at the top in million years (Ma, ages from Müller et al., 2008).
315 ¹GSA Data Repository item 2009xxx, [Please provide a brief description of your data repository
316 items], is available online at www.geosociety.org/pubs/ft2008.htm, or on request from
317 editing@geosociety.org or Documents Secretary, GSA, P.O. Box 9140, Boulder, CO 80301,
318 USA.